EXPERIMENTAL EVALUATION OF SODIUM-TO-AIR HEAT EXCHANGER PERFORMANCE FOR PGSFR DESIGN CODE VALIDATION

S. Yeom*, J. Hong, J. -H. Eoh, J. –M. Kim, Y. Cho, M. -H. Jung, D. -Y. Gam, T. -J Kim, I. Hwang, J. Lee, C. Cho, and J. –Y. Jeong
Korea Atomic Energy Research Institute
111, Daedeok-daero 989beon-gil, Yuseong-gu, Daejeon, 305-353, Republic of Korea
sujin1003@kaeri.re.kr

ABSTRACT

The STELLA program for a PGSFR decay heat removal system (DHRS) performance demonstration is in progress at KAERI. As the first phase of the program, the STELLA-1 facility has been constructed and separate effect tests for the heat exchangers of DHRS have been conducted. A sodium-to-air heat exchanger (AHX), one of the DHRS, was tested for the design code, i.e., AHXSA, verification and validation. In the AHXSA code, Zhukauskas' correlation and Lubarski-Kaufman correlation were used to calculate the heat transfer rate of the AHX at the shell- and tube-side, respectively. Experiments were conducted 23 times with 11 different conditions including the expected operating and design conditions of PGSFR. Air and liquid sodium is introduced into the shell- and tube-side, respectively. After reaching a steady-state, the flow rates and inlet/outlet temperatures of the shell- and tube-side were measured and the total heat transfer rate of the AHX including heat loss was experimentally obtained at the shell- and tube-side. At the tube-side, the measured outlet temperatures and heat transfer rates are consistent with the calculated values using the AHXSA code within 5.6% error range. Furthermore, the dependency of the heat transfer ratio on Richardson number was examined to enhance the reliability of the design code.

KEYWORDS
Air-to-sodium heat exchanger, Decay heat removal, Liquid metal heat transfer

1. INTRODUCTION

According to the long-term fast reactor development plan of the Korean government, a prototype sodium-cooled fast reactor (SFR) will be constructed by 2028. The Korean prototype Gen-Ⅳ SFR(PGSFR) is currently being developed with basic key technologies of KAERI (Korea Atomic Energy Research Institute), which employs highly reliable safety-grade decay heat removal systems. In regard to the verification of decay heat removal performance, a large-scale sodium thermal-hydraulic test program is being carried out. This program is called STELLA (Sodium Test Loop for Safety Simulation and Assessment), and finally aims at the construction of an integral effect test facility subject to the prototype SFR. At the first step of the STELLA program, the first sodium test facility (STELLA-1) was constructed as a separate effect test facility [1].

The STELLA-1 consists of a decay heat removal system (DHRS), a mechanical sodium pump system, and a cold trap system as shown in Figure 1. Among these, the DHRS is a cooling system to protect core from heat damage by removing core decay heat. The DHRS consists of a sodium-to-sodium heat exchanger (DHX) and a sodium-to-air heat exchanger (AHX) and sufficient verification on heat transfer performance is required for safety [2].

The AHX, a passive DHRS (PDHRS), removes heat from the tube-side sodium, which is transferred from the DHX installed in the cold pool of a primary heat transport system (PHTS), to the shell-side outside air. Figure 2 shows a schematic view of the AHX of STELLA-1 and its designed heat removal rate is 1MWt. The AHX is a shell-and-tube type counter-current flow heat exchanger and helically coiled tubes are implemented to accommodate the rapid thermal expansion and contraction. Liquid sodium and air are introduced into the tube- and shell-side, respectively, and the sodium coolant is distributed into 36 branched helical-shaped tubes. In this paper, the heat transfer performance of AHX was tested and the results were compared with design code, i.e. AHXSA, which is developed by KAERI for the design and analysis of the helical-tube type heat exchanger, AHX.

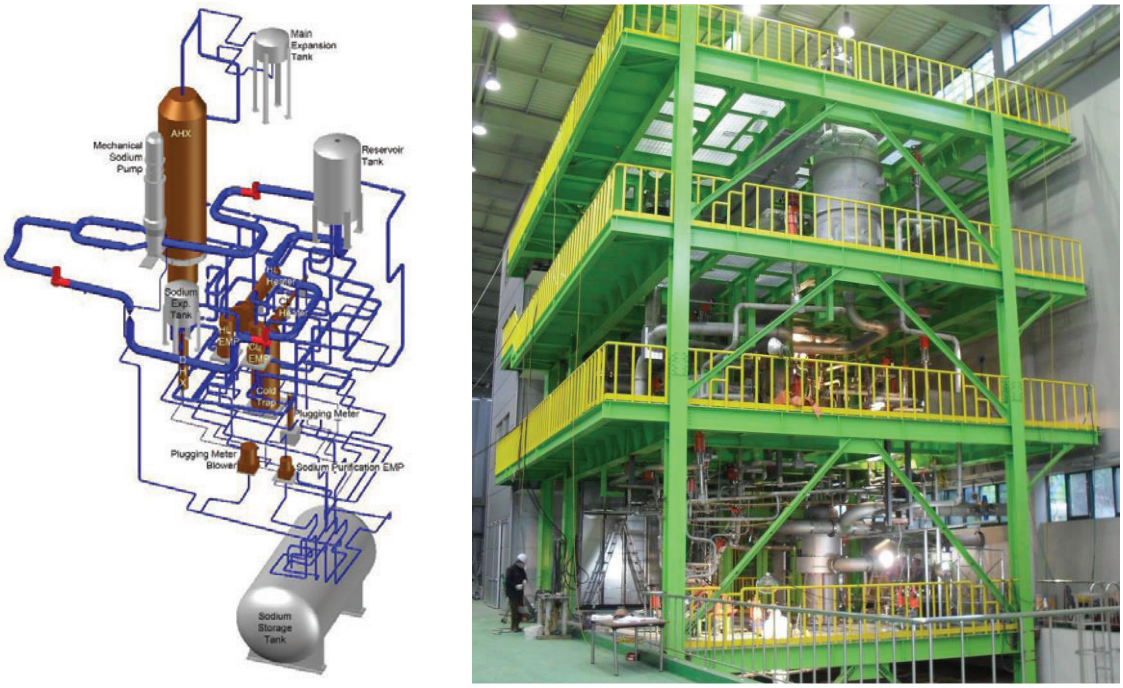

Figure 1. General arrangement of STELLA-1 facility.

Figure 2. Sodium-to-air heat exchanger (AHX) of STELLA-1

2. DESCRIPTION OF THE COMPUTER CODE FOR AHX THERMAL DESIGN

The AHX is designed by using AHXSA code which has been developed for the design and analysis of the helical-tube heat exchanger. A single tube associated with an individual heat transfer tube is basically considered for thermal sizing and the calculation results and design variables regarding heat transfer and pressure drop etc. are reasonably extended to several tubes and tube rows. A single tube is divided into small control volumes and the heat transfer and pressure drop calculations are conducted at each node. Figure 3 shows a schematic diagram of energy balance at a control volume. Energy equations for each control volume can be written as Eqs. (1) ~ (4). Subscripts t and s describe the tube-side and the shell-side, respectively [3].

$$\Delta Q = U \cdot \Delta A_o \cdot \Delta T_{LMTD} \tag{1}$$

$$\Delta Q = w_t \cdot \left(i_{t,in} - i_{t,out}\right) \tag{2}$$

$$\Delta Q = w_s \cdot \left(i_{s,in} - i_{s,out}\right) \tag{3}$$

$$\Delta T_{LMTD} = \left|\left(T_{s,in} - T_{t,in}\right) - \left(T_{s,out} - T_{t,out}\right)\right| \Big/ \ln\left(\frac{T_{s,in} - T_{t,in}}{T_{s,out} - T_{t,out}}\right) \tag{4}$$

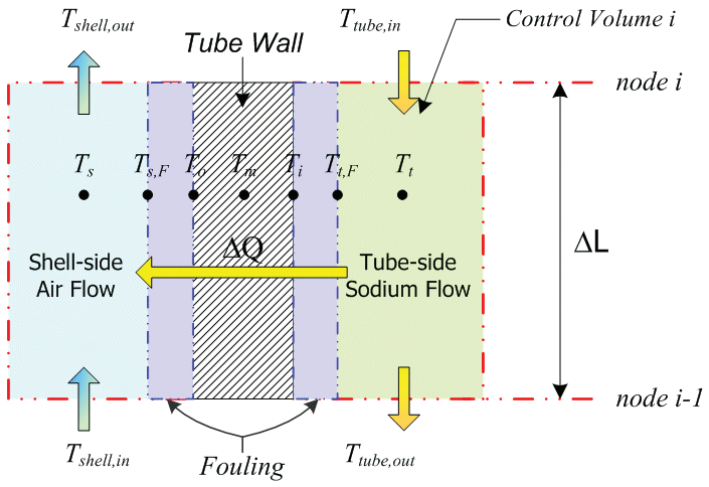

Figure 3. Schematic diagram of energy balance in each control volume

Overall heat transfer coefficient, *U*, is determined by considering the thermal resistances in the heat transfer path, which are determined by the convection resistances of the shell- and tube-side flows, the conduction resistance in the tube wall thickness, and the fouling resistances on the inner and outer surfaces. Based on the energy balance for each heat transfer path, the rate of heat transfer can be written as Eq. (5). By putting Eq. (1) into (5), overall heat transfer coefficient, can be derived as Eq. (6). Temperatures at the inner and outer walls of the heat transfer tube can also be obtained as Eqs. (7) and (8) [3].

$$\begin{aligned}\Delta Q &= h_t \cdot \Delta A_i \cdot \left(T_t - T_{t,F}\right) = h_{t,F} \cdot \Delta A_i \cdot \left(T_{t,F} - T_i\right) \\ &= \Delta A_o \cdot \frac{2 \cdot k}{d_o} \cdot \frac{\left(T_i - T_o\right)}{\ln\left(d_o / d_i\right)} = h_{s,F} \cdot \Delta A_o \cdot \left(T_o - T_{s,F}\right) \\ &= h_{s,F} \cdot \Delta A_o \cdot \left(T_{s,F} - T_s\right)\end{aligned} \tag{5}$$

$$U = \left[\frac{d_o}{d_i} \cdot \frac{1}{h_t} + \frac{d_o}{d_i} \cdot \frac{1}{h_{t,F}} + \frac{d_o}{2 \cdot k} \cdot \ln\left(\frac{d_o}{d_i}\right) + \frac{1}{h_{s,F}} + \frac{1}{h_s}\right]^{-1} \tag{6}$$

$$T_i = T_t - \frac{\Delta Q}{\Delta A_i} \cdot \left(\frac{1}{h_t} + \frac{1}{h_{t,F}}\right) \tag{7}$$

$$T_o = T_s - \frac{\Delta Q}{\Delta A_o} \cdot \left(\frac{1}{h_s} + \frac{1}{h_{s,F}}\right) \tag{8}$$

To calculate heat transfer coefficient at the tube-side sodium, fluid flow inside the tube is assumed to be fully turbulent flow and the forced convection liquid metal heat transfer coefficients, the Lubarski-Kaufman correlation, are used as follows.

$$\mathrm{Nu}_t = 0.625 \cdot \mathrm{Pe}^{0.4} \tag{9}$$

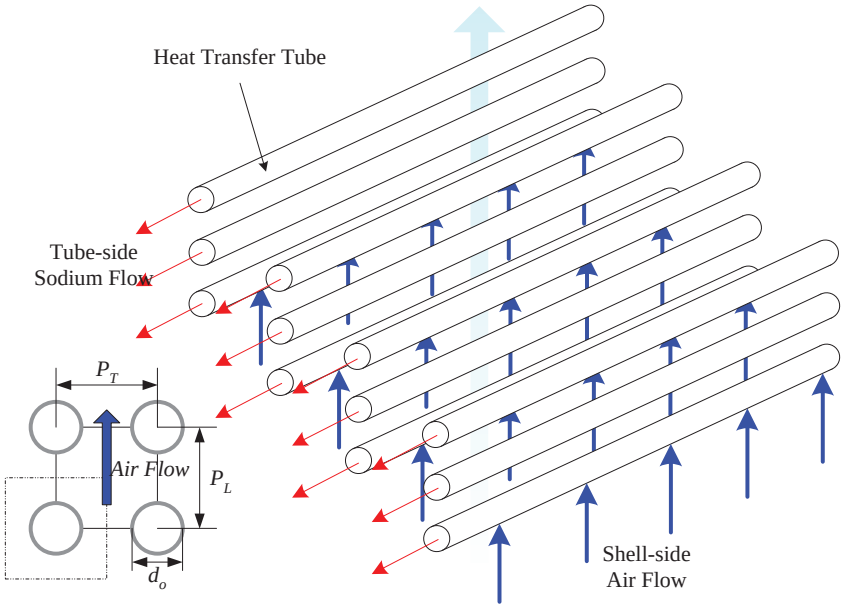

Figure 4. Flow channel model of the AHXSA computer code

For the shell-side air, the helically coiled tube is considered as a tube bundle in cross flow as shown in Figure 4 and Zhukauskas' correlations have been implemented. The open literature was reviewed and multi-dimensional numerical analysis was carried out as well [4, 6].

$$\mathrm{Nu}_s = \xi \cdot \mathrm{Re}_{\mathrm{D,max}}^{m} \cdot \mathrm{Pr}^{0.36} \cdot \left(\frac{\mathrm{Pr}}{\mathrm{Pr}_s} \right)^{0.25} \quad (10)$$

Here, ξ and m are a function of tube bank pitch [5] and $\mathrm{Re}_{\mathrm{D,max}}$ is defined by the maximum velocity of the flow passing the tube bank with the outer diameter of tube as a characteristic length. All the constants used in the correlations are obtained reflecting the characteristics of the staggered and aligned grid arrangements.

3. Experiments

Table I shows experimental conditions of AHX heat transfer performance tests. The tested conditions includes the expected operating conditions of PGSFR as shown in Figure 5.

Table I. Experimental conditions

No.	Flow rate (kg/s)		Inlet temperature (℃)		Note
	Shell (Air)	Tube (Na)	Shell (Air)	Tube (Na)	
1	2.17	2.32	Room temperature	370.2	Repeated for three times.
2	0.47	1.51		377.4	
3	3.00	4.80		450.0	
4	4.58	4.38		370.0	
5	1.04	2.85		374.4	
6	3.58	8.01		386.1	
7	3.50	2.78		455.5	
8	3.50	2.63		406.1	
9	3.50	2.33		330.2	
10	3.00	1.74		357.6	
11	3.00	1.84		395.0	

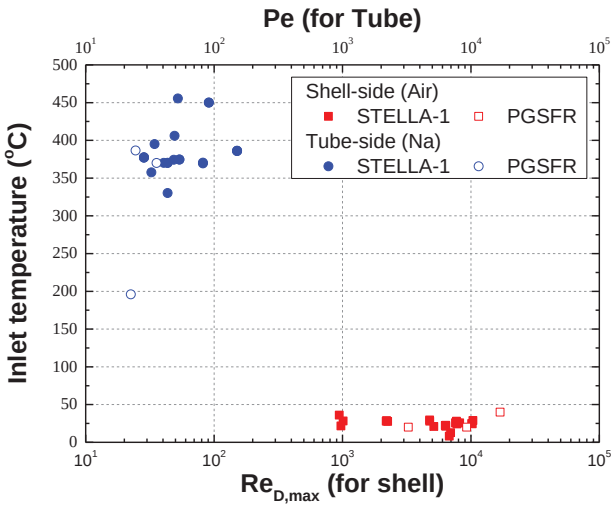

Figure 5. Experimental conditions of STELLA-1 AHX and operating conditions of PGSFR

The sodium was injected into the tubes by the electro-magnetic pump. The flow rate and the inlet temperature were adjusted. Into the shell, the room temperature outside air was injected and flow rate was adjusted by controlling the damper opening and blower power. The shell- and tube-side flow rates and temperatures at the inlet and outlet were collected when the system reaches the steady-state condition, i.e., the fluctuation of sodium flow rate, air flow rate, and temperature are below ±0.1 kg/s, ±0.2kg/s, and ±1℃, respectively, during 10 minutes. The temperatures were measured using K-type thermocouple and the flow rate of the shell- and tube-sides were measured using a thermal mass flow meter and a coriolis flowmeter, respectively. Based on the measured data, the experimentally obtained heat transfer rate was estimated as follows.

$$Q = w \cdot \left| h_{\mathrm{i}}(T_{\mathrm{i}}) - h_{\mathrm{o}}(T_{\mathrm{o}}) \right| \tag{11}$$

The uncertainty of the heat transfer rate was estimated by considering calibration error, DCS system processing error, spatial error, and random error. These factors were applied to each measured values and the total uncertainty, U_{Q}, is obtained by propagating error as Eqs. (12) - (14).

$$B_{\mathrm{Q}} = \sqrt{\left(wh_{\mathrm{i}} \cdot \sqrt{\left(\frac{B_{\mathrm{F}}}{w}\right)^2 + \left(\frac{B_{\mathrm{C_P}}}{C_{\mathrm{P}}}\right)^2 + \left(\frac{B_{\mathrm{T_i}}}{T_{\mathrm{i}}}\right)^2} \right)^2 + \left(wh_{\mathrm{o}} \cdot \sqrt{\left(\frac{B_{\mathrm{F}}}{w}\right)^2 + \left(\frac{B_{\mathrm{C_P}}}{C_{\mathrm{P}}}\right)^2 + \left(\frac{B_{\mathrm{T_o}}}{T_{\mathrm{o}}}\right)^2} \right)^2} \tag{12}$$

$$P_{\mathrm{Q}} = \sqrt{\left(wh_{\mathrm{i}} \cdot \sqrt{\left(\frac{P_{\mathrm{F}}}{w}\right)^2 + \left(\frac{P_{\mathrm{C_P}}}{C_{\mathrm{P}}}\right)^2 + \left(\frac{P_{\mathrm{T_i}}}{T_{\mathrm{i}}}\right)^2} \right)^2 + \left(wh_{\mathrm{o}} \cdot \sqrt{\left(\frac{P_{\mathrm{F}}}{w}\right)^2 + \left(\frac{P_{\mathrm{C_P}}}{C_{\mathrm{P}}}\right)^2 + \left(\frac{P_{\mathrm{T_o}}}{T_{\mathrm{o}}}\right)^2} \right)^2} \tag{13}$$

$$U_{\mathrm{Q}} = \sqrt{B_{\mathrm{Q}}^2 + P_{\mathrm{Q}}^2} \tag{14}$$

4. RESULTS

Figure 6 shows the comparison of working fluid outlet temperatures between experimentally measured values and calculated values using the AHXSA code. For the tube-side sodium, measured values are consistent with the calculated values within 5.6% error range. However, for the shell-side air, calculated values are higher than the measured values throughout the whole data range and the maximum deviation is 8.2%.

Figure 7 shows the comparison of measured and calculated heat transfer rate on the shell- and tube-side. For the tube-side, measured and calculated values are consistent within the range of experimental uncertainty. Maximum deviation is observed at the high heat transfer rate condition and it was 12%. On the other hands, for the shell-side, the calculated values are larger than the measured values as it inferred from Figure 6. Furthermore, the measured heat transfer rates on the shell and tube sides do not match even though the tube-side heat loss is totally transferred to the shell-side. It is inferred that the discrepancy is caused by the humidity of the outside air. Most of experiments were conducted in the humid condition, more than 70% relative humidity. When the humid air is introduced to the shell-side, some of heat, transferred to the air, is applied to the phase change of moisture in the air. Thus, the outlet temperature of shell-side in humid air condition is lower than that in dry air condition. In AHXSA code, applied properties are based on dry air condition. Thus, the calculated values over-predict the measured values.

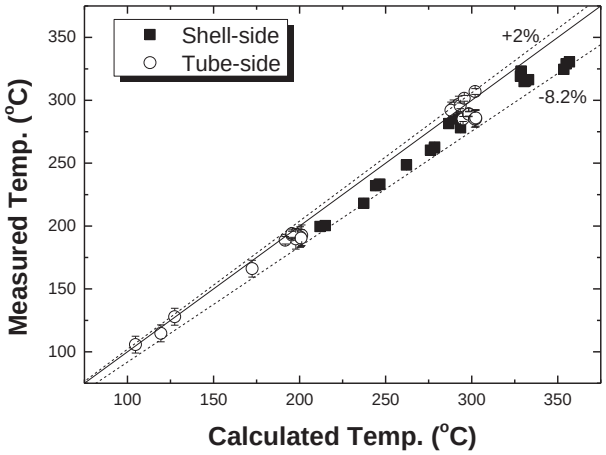

Figure 6. Comparison of outlet temperatures between measured and calculated values.

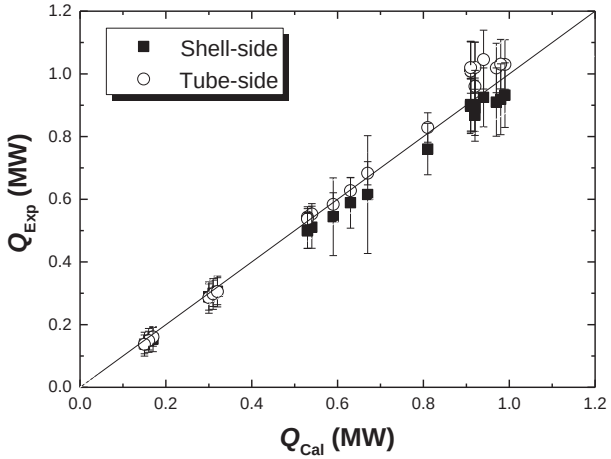

Figure 7. Heat transfer rate of AHX

Figure 8 shows the re-estimated heat transfer rates considering humid air properties. The experimental and calculated values coincide within the uncertainty range. For cases with Q > 0.5MWt, the degree of deviation is reduced from 0.10 for dry air to 0.08 for humid air. Here, the degree of deviation is estimated as Eq. (15). Finally, the difference are reduced by considering the humidity in the air and the experimental results showed good agreement with the calculated results of the AHXSA code.

$$\sigma = \sqrt{\frac{\sum\left(Q_t / Q_s - 1\right)^2}{n}} \tag{15}$$

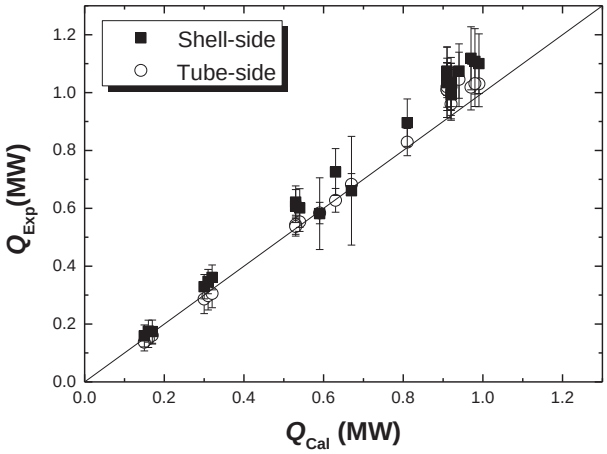

Figure 8. Heat transfer rate of AHX considering humid air condition

5. DISCUSSION

In AHX, most of the thermal resistance, more than 90 %, is caused by the convection heat transfer resistance at the shell-side air. In other word, heat transfer performance is mainly affected by the heat transfer coefficient on the shell-side. As previously described in section 2, the Zukauskas' equation is applied to estimate heat transfer coefficient at the shell-side in the AHXSA code and it is usually used [6] for the helically-coiled tube type heat exchanger, like AHX, in forced convection situations. However, the air flow in the AHX of PGSFR, as a PDHRS, is induced naturally by a chimney effect. In fact, during experiments, only the extent of damper opening rate was controlled instead of controlling the blower for low flow rate conditions. In other words, the air flow is naturally induced at low flow rate conditions in our experiments. Figure 9 shows the theoretical velocity distribution around a tube for the case of forced convection and natural convection. For the forced convection condition, the velocity converges to certain value, *V*, as the distance from the tube surface increases, while the velocity converges to 0 for the natural convection condition. Because of this difference between forced convection and natural convection, it is necessary to consider the suitability of forced convection heat transfer coefficient to the natural convection condition.

(a) Forced convection flow **(b) Natural convection flow**

Figure 9. Velocity distribution around tube

Figure 10 (a) shows the tendency of the heat transfer ratios between measured and calculated values. At the low heat transfer rate, the calculated values over-predict the experimental values. As the heat transfer

rate increases, namely the flow rate or temperature difference between inlet and outlet increases, the ratio gets larger. Thus, it is examined that the experimented ranges are suitable to use forced convection correlation as shown in the Figure 10 (b). In general, Richardson number (Ri) is a non-dimensionalized number used to characterize the relative importance of convection condition and it is defined as Eq. (16) [5]. When Ri is larger than 1, natural convection is dominant and it approaches to 1, both natural convection and forced convection should be considered.

$$\mathrm{Ri_L} = \frac{\mathrm{Gr}}{\mathrm{Re}} = \frac{g\beta(T_s - T_\infty)L}{V^2} \tag{16}$$

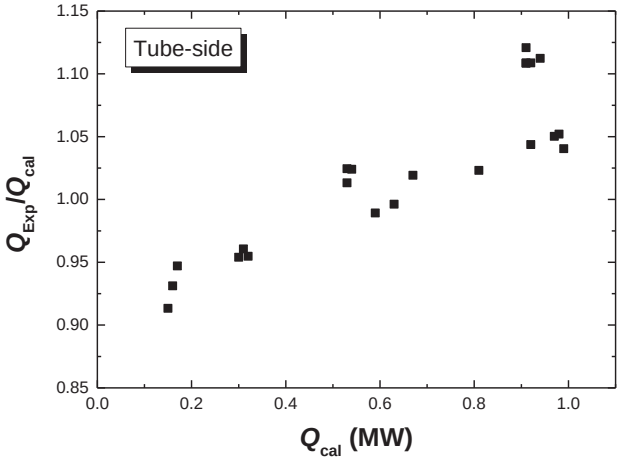

(a) The dependency on heat transfer rate

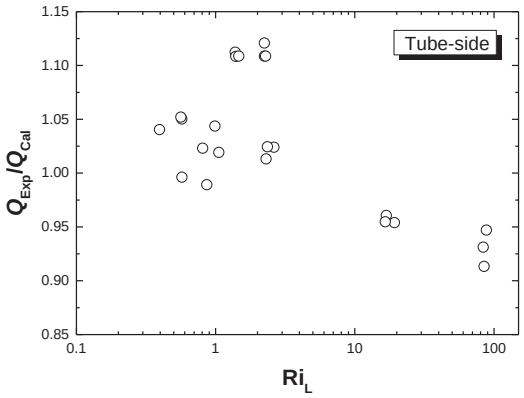

(b) The dependency on Richardson number

Figure 10. The dependency of the heat transfer rate ratio between experiments and calculations.

As shown in Figure 10 (b), the value of Ri varies from 0.39 to 89 in the entire tested range and this corresponds to the range where natural convection should be considered. When the $\mathrm{Ri_L}$ is smaller than 3, the heat transfer ratio is larger than 1. This means that the experimental value is larger than the calculated value and some factors, such as natural convection, should be considered to enhance heat transfer

coefficient. When the Ri is larger than 10, the experimental value is smaller than the calculated value. It seems that the excessive heat transfer coefficient is used because of forced convection assumption although the experimented range is natural convection condition. Thus, the heat transfer coefficient at the shell-side should be modified to reflect the effect of natural convection in future work

6. CONCLUSIONS

In this paper, the heat transfer performance tests were conducted at the 1MWt sodium-to-air heat exchanger (AHX) and the results was compared with a design code, i.e. AHXSA. As a result, the experimental values and calculated values coincide within uncertainty ranges. Furthermore, to enhance the reliability of design code, the dependency of the heat transfer ratio between the experiments and calculations is examined with the non-dimensionalized number, i.e. Ri. Finally, it is suggested as a future work that the natural convection effect should be considered on the heat transfer coefficient at the shell-side.

NOMENCLATURE

Notation	Description	Unit
A	Area	m^2
B_Q	Bias error	-
c_p	Specific heat	kJ/kg·K
d	diameter	m
h	Convective heat transfer coefficient	$W/m^2 \cdot K$
i	Enthalpy	kJ/kg
k	Coefficient of thermal conductivity	W/m·K
L	Height of tube bundle	m
Nu	Nusselt number	-
P_Q	Precision error	-
P_T	Transverse pitch of tube bundle	m
Pe	Peclet number	-
Pr	Prandtl number based on fluid temperature	-
Pr_s	Prandtl number based on surface temperature	-
Q	Heat transfer rate	W
Re_D	Reynolds number with tube diameter as a chracteristic length	-
$Re_{D,max}$	Reynolds number with maximum velocity at tube bundle, $\frac{\rho D}{\mu}\frac{P_T}{P_T - d_o}V$	-
Ri	Richardson number	-
T	Temperature	K
ΔT_{LMTD}	Log-mean temperature difference ,	K
U	Overall heat transfer coefficient	$W/m^2 \cdot K$
U_Q	Total uncertainty	-
V	velocity	m/s
w	Mass flow rate	Kg/s
Subscript		
F	Fouling	
i	Inner side	
in	Inlet	
o	Outer side	
out	Outlet	

s	Shell-side	
t	Tube-side	

ACKNOWLEDGMENTS

This work was supported by the National Research Foundation of Korea (NRF) grant funded by the Korea government (MSIP). (No. 2012M2A8A2025635)

REFERENCES

1. J. H. Eoh, H.Y. Lee, T.J. Kim, J.Y. Jeong, and Y.B. Lee, "Design Features of a Large-scale Sodium Thermal-hydraulic Test Facility: STELLA," *International Conference on Fast Reactors and Related Fuel Cycles (FR13)*, Mar. 3–8, Paris, France (2013).
2. J. –H. Eoh, H. –Y. Lee, T. –J. Kim, J. –Y Jeong, and Y. –B. Lee, " Design and construction of the sodium thermal hydraulic experimental facility : STELLA-1," *The 18th Pacific Basin Nuclear Conference (PBNC 2012)*, Bexco, Busan, Korea, March 18~23, PBNC 2012-KA0151(2012).
3. J. Hong, "AHX sizing calculation," *Korea Atomic Energy Research Institute*, SFR-513-DF-302-001 (2014)
4. H. C. Kang, J. -H. eoh, J. –E. Cha, and S. –O. Kim, "Numerical study on pressure drop and heat transfer for designing sodium-to-air heat exchanger tube banks on advanced sodium-cooled fast reactor," *Nucl. Eng. Des.* 254, pp.5-15 (2013)
5. F. P. Incropera and D. P. DeWitt, " Fundamentals of heat and mass transfer," John Wiley & Sons (2002)
6. Y. Inagaki, H. Koiso, H. Takumi, I. Ioka, and Y. Miyamoto, "Thermal hydraulic study on a high-temperature gas-gas heat exchanger with helically coiled tube bundles," *Nucl. Eng. Des.* 185, pp. 141-151 (1998).